frontiers in Materials

ORIGINAL RESEARCH
published: 16 November 2021
doi: 10.3389/fmats.2021.761052

The Pilling-Bedworth Ratio of Oxides Formed From the Precipitated Phases in Magnesium Alloys

Quantong Jiang[1,2,3]*, Dongzhu Lu[1,2,3], Chang Liu[1,2,3], Nazhen Liu[1,2,3]* and Baorong Hou[1,2,3]

[1]CAS Key Laboratory of Marine Environmental Corrosion and Bio-Fouling, Institute of Oceanology, Chinese Academy of Sciences, Qingdao, China, [2]Open Studio for Marine Corrosion and Protection, Pilot National Laboratory for Marine Science and Technology (Qingdao), Qingdao, China, [3]School of Materials Science and Engineering, Qilu University of Technology, Jinan, China

The Pilling-Bedworth ratio of oxides preferentially formed from the precipitated phases in magnesium alloys were calculated. The results showed that the PBR value of Nd_2O_3 preferentially formed from $Mg_{12}Nd$ was 1.0584, and the PBR value of Y_2O_3 preferentially formed from $Mg_{24}Y_5$ was 1.1923. Both the Nd_2O_3 and Y_2O_3 would provide a good protection to the Mg matrix. The Gd_2O_3 preferentially formed from Mg_3Gd, whereas the MgO preferentially formed from $MgNi_2$. The PBR value of these two oxides were both larger than 2. The corresponding oxides formed from the common precipitated phases $Mg_{17}Al_{12}$, $MgZn_2$, $MgCu_2$, Mg_2Ca, $Mg_{12}Ce$, and MgAg were all less than 1. The oxide films formed on surfaces of pure Mg and Mg-xY (x = 3, 5, 7 wt.%) alloys at high temperatures were analyzed. The results showed that the oxide films were composed of a Y_2O_3/MgO outer layer and an inner layer rich with Y_2O_3. The formation of Y_2O_3 was mainly caused by the oxidation of $Mg_{24}Y_5$. The more Y_2O_3 existed in the composite oxidation film, the better corrosion resistance of the Mg-Y samples.

Keywords: oxide, PBR value, magnesium alloys, precipitated phases, Mg-Y

Edited by:
Yingwei Song,
Institute of Metals Research (CAS), China

Reviewed by:
Jun Chen,
Xihua University, China
Fuyong Cao,
Xiamen University, China

****Correspondence:***
Quantong Jiang
jiangquantong@qdio.ac.cn
Nazhen Liu
liunazhen@qdio.ac.cn

Specialty section:
This article was submitted to Structural Materials, a section of the journal Frontiers in Materials

Received: *19 August 2021*
Accepted: *08 October 2021*
Published: *16 November 2021*

Citation:
Jiang Q, Lu D, Liu C, Liu N and Hou B (2021) The Pilling-Bedworth Ratio of Oxides Formed From the Precipitated Phases in Magnesium Alloys. Front. Mater. 8:761052. doi: 10.3389/fmats.2021.761052

INTRODUCTION

The PBR (Pilling-Bedworth Ratio) value of oxide film is an important parameter to evaluate the film protection performance to the base metal (Xu and Gao, 2000). When the PBR value is less than 1, the protection performance of the oxide film is poor, due to the existing tensile stress and the resultant incomplete coverage of the oxide film to the metal. Similarly, when the PBR value is larger than 3, the oxide film also shows a weak protection, due to the compressive stress in the film. When the PBR value is between 1 and 2, the oxide film is protective (Bradford 1993; Tan et al., 2016; Song et al., 2021).

Magnesium is active, so the α-Mg matrix and precipitated phases in magnesium alloys are prone to be oxidized in the atmospheric environment (Czerwinski 2002; Liu et al., 2009; Medved et al., 2009), leading to the formation of different kinds of oxidation films on the magnesium alloy surface (Czerwinski, 2012; Czerwinski, 2015). The PBR value of oxidation film formed on pure magnesium is about 0.8, which is not protective (You et al., 2000; Mebarki et al., 2005; Cheng et al., 2009; López et al., 2010).

There are many precipitated phases existing in magnesium alloys, including $Mg_{17}Al_{12}$, $MgZn_2$, Mg_2Ca, Mg_5Gd, $Mg_{12}Nd$ and $Mg_{24}Y_5$, etc., (Nie 2012; Zhu and Chen, 2019; Kaya, 2020; Shi et al., 2020). The crystallography of the precipitated phases determines the microstructure and property of magnesium alloys. According to the literatures, the film formed by oxidation of precipitated phases during the heat treatment process, has good corrosion resistance (Sudholz et al., 2011; Chang et al.,

TABLE 1 | Absolute atomic mass of different alloying elements.

Atomic species	C^{12}	Mg	Al	Zn	Cu	Ca
Relative mass	12.017	24.305	26.982	65.409	63.546	40.078
Absolute mass/10^{-26}Kg	1.9927	4.0303	4.4742	10.846	10.537	6.6450
Atomic species	**Gd**	**Nd**	**Ce**	**Ag**	**Ni**	**Y**
Relative mass	157.25	144.242	140.116	107.868	58.693	88.905
Absolute mass/10^{-26}Kg	26.0757	23.9187	23.2345	17.887	9.733	14.7425

2015; Yu et al., 2015). Due to the different activity of alloying elements, the property of oxide film formed from the precipitated phases in the atmospheric environment is different (Van Orman and Crispin, 2010). PBR is the ratio of oxide volume consisting metal and oxygen on the metal surface, to the volume of base metal atoms, which reflects the stress condition in the oxide film. The corrosion tendency of magnesium alloy is closely related to the conditions of the oxide layer (Wang et al., 2007; Fan et al., 2011).

In this work, the PBR values of oxides formed from the precipitated phases in magnesium alloys were calculated. In order to verify the PBR calculation results of oxides formed from the precipitated phases in magnesium alloys, the morphologies of oxidation films formed on the surfaces of pure Mg and Mg-xY alloys (x = 3, 5, 7 wt.%) at high temperature were characterized. The effect of the oxidation films on corrosion resistance were also studied. This work is expected to give a scientific and reasonable method to improve intrinsic corrosion resistance of magnesium alloys by regulating the types of precipitates.

CALCULATION OF THE PILLING-BEDWORTH RATIO VALUE

Calculation of Absolute Atomic Mass

The relative atomic mass values of the alloying elements, including Al,Zn, Cu, Ca, Gd, Nd, Ce, Ag, Ni, Y and C^{12} were obtained from the periodic table of elements. The absolute atomic mass values of the alloying elements were calculated via the following formula:

$$Absolute\ tomic\ mass = \frac{Relative\ atomic\ mass\ of\ \ alloying\ elements}{Relative\ atomic\ mass\ of\ C12} \times 1.9927 \times 10^{-26} Kg \tag{1}$$

The results were shown in **Table 1**.

Molar Volume of Precipitated Phases Mg_AX_B in Magnesium Alloys

The crystal structure and parameters of the common precipitated phases in the magnesium alloys, including $Mg_{17}Al_{12}$, $MgZn_2$, $MgCu_2$, Mg_2Ca, Mg_3 Gd, $Mg_{12}Nd$, $Mg_{12}Ce$, MgAg, $MgNi_2$ and $Mg_{24}Y_5$ were obtained by the phase diagram.

The atom number in a single unit cell of the precipitated phases Mg_AX_B was calculated via the crystal structure. For example, the crystal structure of $Mg_{24}Y_5$ is body-centered cubic (BCC), so there are two $Mg_{24}Y_5$ intermetallics in each unit cell. The total atom number in a single $Mg_{24}Y_5$ unit cell is 2 × (24Mg+5Y) = 48Mg + 10Y. The absolute mass of a single $Mg_{24}Y_5$ unit cell (the sum of 48Mg atoms and 10 Y atoms) was obtained as following: $48 \times 4.0303\times10^{-23}$ g + $10 \times 14.7425 \times 10^{-23}$ g = 340.8794×10^{-23} g. The absolute mass of other single precipitated phases Mg_AX_B was calculated via the same method with results shown in **Table 2**.

The volume of a single unit cell was calculated according to the crystal structure and parameters obtained from the XRD card. The density of a single unit cell was calculated via the following formula:

$$Density\ of\ a\ \ single\ unit\ cell = \frac{Absolute\ mass\ of\ a\ single\ unit\ cell}{Volume\ of\ a\ single\ unit\ cell} \tag{2}$$

The $Mg_{24}Y_5$ unit cell is body-centered cubic (BCC) structure, and the lattice parameters is a = 1.1257×10^{-7} cm. So the Volume of a single unit cell is $a^3 = (1.1257 \times 10^{-7}\,cm)^3 = 1.4265 \times 10^{-21}\,cm^3$, the density of a single $Mg_{24}Y_5$ unit cell is $\frac{340.8794\times10^{-23}g}{1.4265\times10^{-21}cm^3} = 2.3896/cm^3$, according to **Eq. 2**. The densities of single unit cells of the other precipitated phases were obtained via the same method. The density of a single $Mg_{24}Y_5$ unit cell is the density of the $Mg_{24}Y_5$ intermetallics.

The molar volume of precipitated phases Mg_AX_B in magnesium alloys was calculated via the formula as follow:

$$Molar\ volume\ of\ \ precipituated\ phases = \frac{Molarmassofprecipitatedphases}{DensityofasingleMgAXBunitcell} \tag{3}$$

For example, the molar volume of $Mg_{24}X_5\frac{1027.845}{2.3896} = 430.132\,cm^3$. All the calculated results are shown in **Table 2**.

Pilling-Bedworth Ratio Calculation of Oxidation Formed From Precipitated Phases

According to the formation Gibbs energies of the metal's oxides (James 2005), the preferential metal atom of the precipitated

TABLE 2 | Molar volume of precipitated phases Mg_AX_B in magnesium alloys.

Precipitated phases	Crystal structure	A single unit cell of precipitated phases MgAXB					Molar mass	Molar volume
		Number of atoms	Mass/ 10^{-23}g	Lattice parameters	Volume 10^{-21}cm^3	Density g/cm^3		
$Mg_{24}Y_5$	BCC	48+10	340.8794	a = 1.1257	1.4265	2.3896	1,027.845	430.132
Mg_3Gd	FCC	12+4	152.6664	a = 0.7326	0.3932	3.8828	230.165	59.2781
$Mg_{12}Ce$	BCC	24+2	143.1962	a = 1.033 c = 0.5964	0.6364	2.2501	431.776	191.892
$Mg_{12}Nd$	BCC	4+2	144.5646	a = 1.031 c = 0.593	0.6303	2.297	435.902	189.770
$Mg_{17}Al_{12}$	BCC	34+24	244.411	a = 1.056	1.1776	2.078	736.969	354.653
$MgZn_2$	HCP	2+4	51.4458	a = 0.5222 c = 0.8568	0.6075	4.960	155.123	31.275
$MgCu_2$	FCC	4+8	100.4204	a = 0.7048	0.3415	5.745	151.397	25.880
Mg_2Ca	HCP	4+2	29.4130	a = 0.623 c = 1.012	1.0212	1.732	88.688	51.206
MgAg	SC	1+1	21.9173	a = 0.3314	0.0364	6.030	132.173	21.919
$MgNi_2$	HCP	2+4	46.9914	a = 0.4824 c = 1.5826	0.9575	5.902	107.303	18.181

phases Mg_AX_B in magnesium alloys during oxidation reaction in the atmospheric environment were:

1) $\Delta_fG^\circ Al_2O_3 = -38.5$ kJ/mol > $\Delta_fG^\circ MgO = -135.27$ kJ/mol; $Mg_{17}Al_{12} \rightarrow Mg \rightarrow MgO$
2) $\Delta_fG^\circ ZnO = -76.08$ kJ/mol > $\Delta_fG^\circ MgO = -135.27$ kJ/mol; $MgZn_2 \rightarrow Mg \rightarrow MgO$
3) $\Delta_fG^\circ CuO = -31.0$ kJ/mol > $\Delta_fG^\circ MgO = -135.27$ kJ/mol; $MgCu_2 \rightarrow Mg \rightarrow MgO$
4) $\Delta_fG^\circ CaO = -144.25$ kJ/mol < $\Delta_fG^\circ MgO = -135.27$ kJ/mol; $Mg_2Ca \rightarrow Ca \rightarrow CaO$
5) $\Delta_fG^\circ Gd_2O_3 = -434.9$ kJ/mol < $\Delta_fG^\circ MgO = -135.27$ kJ/mol; $Mg_3Gd \rightarrow Gd \rightarrow Gd_2O_3$
6) $\Delta_fG^\circ Nd_2O_3 = -411.3$ kJ/mol < $\Delta_fG^\circ MgO = -135.27$ kJ/mol; $Mg_{12}Nd \rightarrow Nd \rightarrow Nd_2O_3$
7) $\Delta_fG^\circ Ce_2O_3 = -407.80$ kJ/mol < $\Delta_fG^\circ MgO = -135.27$ kJ/mol; $Mg_{12}Ce \rightarrow Ce \rightarrow Ce_2O_3$
8) $\Delta_fG^\circ Ag_2O = -2.68$ kJ/mol > $\Delta_fG^\circ MgO = -135.27$ kJ/mol; $MgAg \rightarrow Mg \rightarrow MgO$
9) $\Delta_fG^\circ NiO = -50.6$ kJ/mol > $\Delta_fG^\circ MgO = -135.27$ kJ/mol; $MgNi_2 \rightarrow Mg \rightarrow MgO$
10) $\Delta_fG^\circ Y_2O_3 = -434.19$ kJ/mol < $\Delta_fG^\circ MgO = -135.27$ kJ/mol; $Mg_{24}Y_5 \rightarrow Y \rightarrow Y_2O_3$

If there is one type of precipitated phase A_UB_V in magnesium alloy, the preferentially oxidized element is B-content in the A_UB_V single unit cell. Because the preferentially oxidized B-content is derived from A_UB_V, which is a solid solution structure. Therefore, the volume of B-content can be obtained from the volume of A_UB_V single unit cell subtracted the volume of unoxidized A-content (Xu and Gao, 2000), as shown by the following formula,

$$Volume\,of\,x_B = Volume\,of\left[(\mathbf{X/V})_{\mathbf{AuBv}}\right] - Volume\,of\left[(ux/v)_A\right] \tag{4}$$

For example, the molar volume of Y atom in $Mg_{24}Y_5$ unit cell was calculated via: $1/5\left[V_{Mg_{24}Y_5} - 24V_{Mg}\right] = 1/5 \times [430.132 - 24 \times 13.9845]\text{cm}^3 = 18.9008\ \text{cm}^3$. In consideration of x in **Eq. 6** (2 for Y_2O_3), the volume of 2 mol of Y in alloy is calculated by $2 \times 18.9008\ \text{cm}^3 = 37.8016\ \text{cm}^3$.

Then, the density and molar mass of oxide product can be obtained via periodic table of elements. Thus, the molar volume of oxidized product can be calculated via the formula:

$$Molarvolumeo\,f\,oxide = \frac{Molarmasso\,f\,oxideproduct}{Densit\,yo\,f\,oxideproduct} \tag{5}$$

For example, the molar volume of oxide product Y_2O_3 from the oxidation of precipitated phases $Mg_{24}Y_5$ was calculated as follow: $\frac{M_{Y_2O_3}}{D_{Y_2O_3}} = \frac{225.81\ g/\text{mol}}{5.01\ g/\text{cm}^3} = 45.0719$.

The PBR value of oxidation films formed from the precipitated phases in magnesium alloys was calculated via the formula:

$$PBR_{\text{precipitated phases}}\,\frac{Volumeo\,f\,onemoleo\,f\,B_xO_y}{Volume\,o\,f\,x\,moles\,o\,f\,B\,in\,\,alloy} \tag{6}$$

All the results were shown in **Table 3**.

Characteristic of Oxide Films on the Mg-xY (x = 3, 5, 7 wt.%) Alloys Surfaces

Commercially pure Mg (99.9 wt. %), Mg- 3Y wt.%, Mg- 5Y wt.% and Mg- 7Y wt.% were used to characterize the oxide film on the surface of magnesium alloys. The samples with dimensions of 1 cm × 1 cm×1 cm were heated in the dry air at 400°C for 36 h. These samples were used to analyze the microstructure of oxide films, including the morphologies, thicknesses and compositions by scanning electron microscopy (SEM) and energy dispersive spectroscopy (EDS). The samples with dimensions of 2 cm × 2 cm × 0.5 cm were also heated in dry air at 400°C for 36 h, which were used to test the open circuit potential (OCP) using the electrochemical workstation. Three parallel samples were used to ensure the accuracy of the test results. All the samples were polished with 1,000, 3,000 and 5,000# SiC papers and then cleaned with absolute ethanol.

Due to the affinity of oxygen to magnesium alloys, samples are oxidized rapidly at a high temperature in dry air. The rate of oxidation increases first linearly, then exponentially with the

TABLE 3 | PBR value of the oxide film formed from the precipitated phases of magnesium alloys.

Precipitated phases Mg_AX_B in magnesium alloys	Mg_AX_B Volume/cm^3	The lower metal activity element in Mg_AX_B		The molar volume of the preferentially oxidized metal/cm^3	Preferentially oxidized product			PBR value of oxidation films formed from Mg_AX_B
		Density (g/cm3)	Volume/ cm^3		Molar mass	Density g/cm^3	Volume/ cm^3	
$Mg_{24}Y_5$	430.132	Mg = 1.738	13.9845	Y = 37.8016	Y2O3 = 225.81	5.01	45.0719	1.1923
Mg_3Gd	59.2781	Mg = 1.738	13.9845	Gd = 17.3246	Gd2O3 = 362.49	7.41	48.9201	2.8237
$Mg_{12}Ce$	191.892	Mg = 1.738	13.9845	Ce = 48.156	Ce2O3 = 328.24	7.13	46.0365	0.9560
$Mg_{12}Nd$	189.770	Mg = 1.738	13.9845	Nd = 43.912	Nd2O3 = 336.47	7.24	46.4738	1.0584
$Mg_{17}Al_{12}$	354.653	Al = 2.70	9.9933	Mg = 13.8078	MgO = 40.304	3.65	11.042	0.7997
$MgZn_2$	31.275	Zn = 7.14	9.1609	Mg = 12.9532	MgO = 40.304	3.65	11.042	0.8525
$MgCu_2$	25.880	Cu = 8.96	7.0922	Mg = 11.6956	MgO = 40.304	3.65	11.042	0.9441
Mg_2Ca	51.206	Mg = 1.738	13.9845	Ca = 23.237	CaO = 56.077	3.25	17.254	0.7425
MgAg	21.919	Ag = 10.49	10.2829	Mg = 11.429	MgO = 40.304	3.65	11.042	0.9661
$MgNi_2$	18.181	Ni = 8.908	6.5888	Mg = 5.0034	MgO = 40.304	3.65	11.042	2.2069

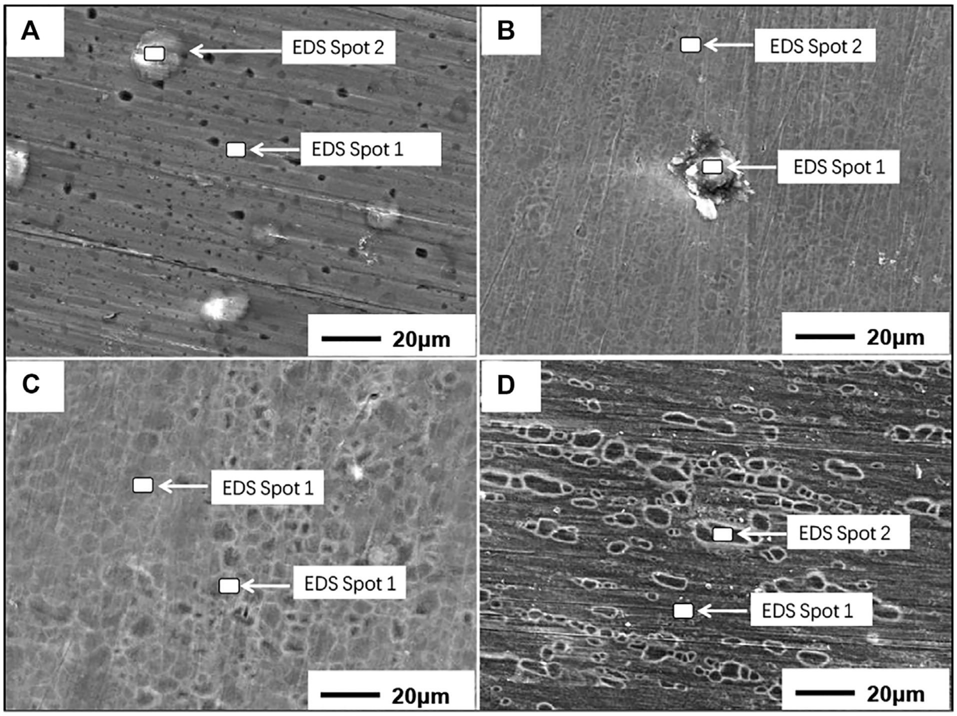

FIGURE 1 | The oxides morphologies of different samples: **(A)** pure Mg; **(B)** Mg-3Y; **(C)** Mg-5Y; **(D)** Mg-7Y.

extension of oxidation time (Zhou et al., 2013; Yu et al., 2016). Below 400–450°C, the magnesium alloys have certain oxidation resistance, with a parabolic oxidation kinetics and intact oxide film (Yu et al., 2018). Once the temperature exceedes 400°C, the oxidation reaction kinetics will change from parabolic to linear. The acceleration of oxidation reaction leads to the formation of film cracks on the surface. Therefore, in order to study the microstructure of the dense oxide films on Mg-Y alloys, the oxidation temperature of 400°C was chosen. The thermo gravimetric analysis (TGA) was used to measure the weight increment of different samples. The heating rate was 10°C/min in the air environment from room temperature to 500°C.

As shown in **Figure 1**, the morphologies of oxide films formed on Mg-xY (x = 0, 3, 5, 7 wt.%) samples are quite different. Many MgO particles and pores existed on the surface of pure Mg, indicating a poor corrosion resistance of the oxide film. With the addition of 3 wt.% Y, the surface tended to be smooth and compact, and the pores were also disappeared. However, there

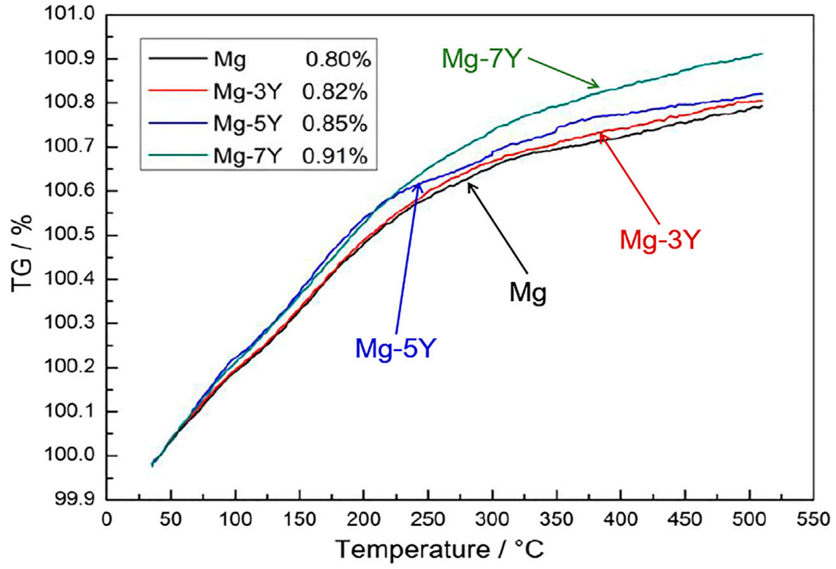

FIGURE 2 | The thermo gravimetric analysis results of different samples.

TABLE 4 | The EDS results of oxides of different materials.

Materials	**Locations**	**Weight %**		
		Element Mg *K*	**Element O *K***	**Element Y *K***
Mg	Spot 1	98.4	1.6	—
	Spot 2	95.6	4.4	—
Mg-3Y	Spot 1	71.5	15.6	12.8
	Spot 2	60.2	21.7	18.1
Mg-5Y	Spot 1	64.0	17.2	18.7
	Spot 2	53.0	22.5	24.5
Mg-7Y	Spot 1	57.0	21.4	21.6
	Spot 2	55.6	23.2	21.2

TABLE 5 | The EDS mapping analysis of different samples.

Materials	**Locations**	**Weight %**		
		Element Mg *K*	**Element O *K***	**Element Y *K***
Mg	mapping	97.5	2.5	—
Mg-3Y	mapping	65.1	13.8	21.1
Mg-5Y	mapping	62.1	14.1	23.8
Mg-7Y	mapping	57.0	16.1	26.9

were still a small amount of MgO particles on the sample surface. With the increasing of Y-content, MgO particles disappeared completely, whereas the squama-like oxides formed on the surface of Mg-5Y alloys. As the Y content increased to 7 wt.%, the size of the squama-like oxides becomes larger, and the boundary of oxides turned clearly.

The EDS results of oxides on the surface of Mg-xY (x = 0, 3, 5, 7 wt.%) samples are shown in **Table 4**. The Y-contents in the oxides are more than the matrix. Both the O-content and Y-content increased with the addition of Y element, whereas the Mg-content decreased. This phenomenon because that the activity of Y element is higher than Mg element. With the extension of oxidation time, the thickness of oxides increased. The oxidation rate of all the samples was reduced by the oxides barrier, which inhibited the inward diffusion of O_2 and the outward diffusion of Mg^{2+}. According to the calculation in **Table 3**, the PBR of Y_2O_3 formed from the $Mg_{24}Y_5$ unit cell was 1.1923, which indicated that the Y_2O_3 oxidation film was compact. Moreover, the chemical property of Y_2O_3 was relatively stable. Therefore, when Mg-Y alloys were exposed in the high temperature environment, the dense MgO/Y_2O_3 composite oxide layers were formed on the sample surfaces. The composite oxide layer acted as a physical barrier to hinder the oxidation reaction, thus the oxidation of magnesium alloys was slowed down (Wang et al., 2008).

The TGA result was shown in **Figure 2**. From the trends of the curves in the figure, all samples had a fast oxidation rate at the initial stage. The oxidation reaction rate decreased with the prolong of oxidation reaction time and the rising of temperature. The Mg-5Y alloys had the faster oxide reaction rate than the pure Mg, Mg-3Y and Mg-7Y samples at the initial stage of oxidation. Then, the thin, smooth and dense oxide films were formed on the surface of samples, the oxidation rates were all reduced. At the maximum temperature, the weight improvement ratio of pure Mg, Mg-3Y, Mg-5Y and Mg-7Y was 0.80, 0.82, 0.85 and 0.91%, respectively. This phenomenon indicated that Y element had the higher activity to bind with oxygen than Mg.

According to the mapping results in **Figure 3**, the difference of Y-content in Mg-xY (x = 3, 5, 7 wt.%) alloys led to the different elementary composition in the oxidation products.

As shown in **Table 5**, mapping analysis on the surface of pure magnesium showed that the O content was only 2.5%. This

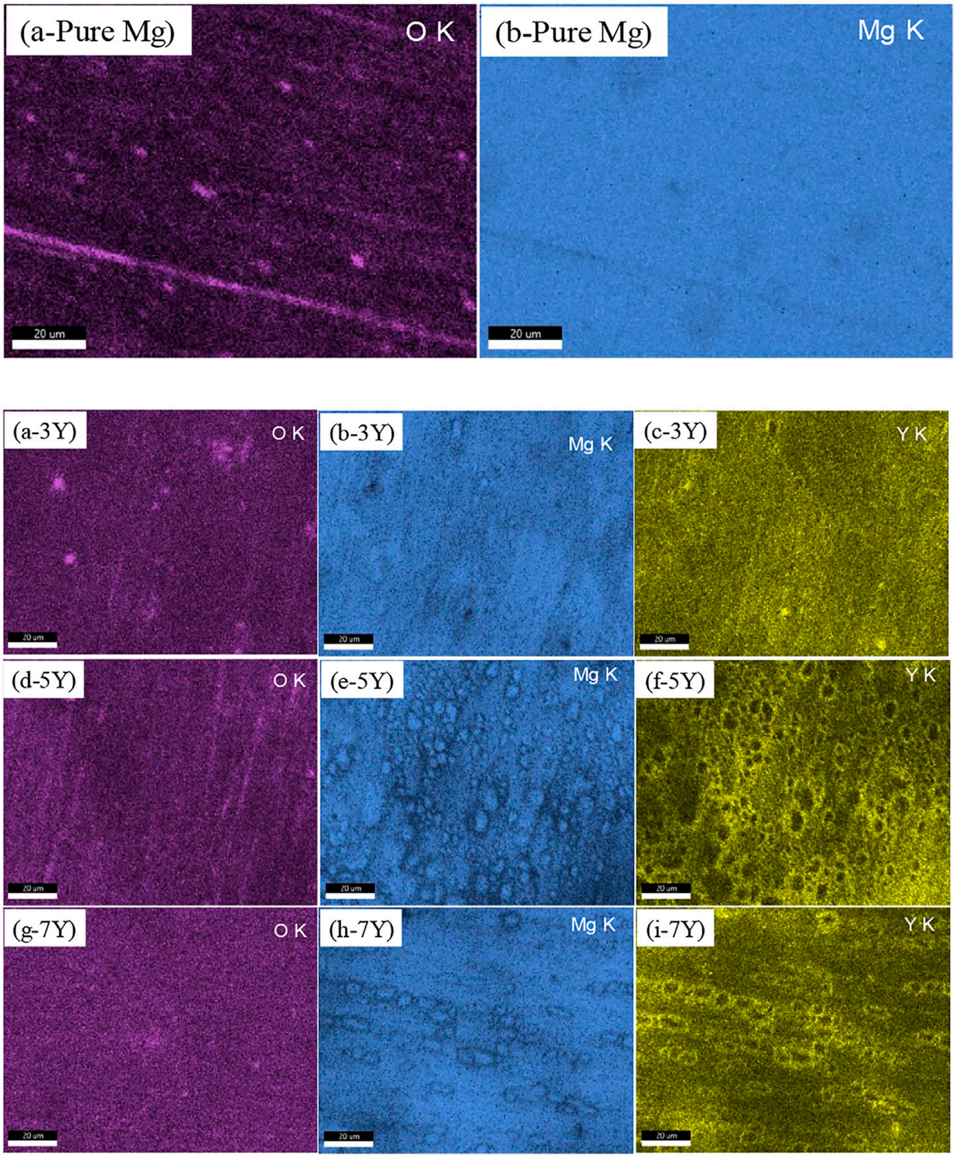

FIGURE 3 | The mapping results of elementary composition in the oxidation products on different samples surfaces: (a-pure Mg) and (b-pure Mg): pure Mg; (a-3Y) and (b-3Y) and (c-3Y): Mg-3Y; (d-5Y) and (e--5Y) and (f-5Y): Mg-5Y; (g-7Y) and (h-7Y) and (i-7Y): Mg-7Y.

phenomenon proved that the oxide film on the surface was very thin, so that the electron beam can penetrate the oxide film and reach the Mg matrix. The oxidation films of Mg-3Y samples were composed of MgO as the major constituent and minor Y_2O_3. When Y-content was 3 wt.%, the average content of oxygen element in the surface mapping analysis was about 13.8 wt.%, and the Y element was about 21.1 wt.%, which indicated that a large number of Y_2O_3 were formed in the oxide film. The content of Y element was larger than that of in the alloy matrix without oxidation. With the increase of Y-content to 7 wt.%, the O element on the surface film increased to 16.1 wt.%, while the Y content increased to 26.9 wt.%.

The average thicknesses of oxidation films for different samples were measured by backscattered electrons scanning spectroscopy, as shown in **Figure 3**. And the elemental composition at different cross-section locations was also analyzed by EDS, with results summarized in **Table 6**. In **Figure 4** the average thickness of oxidation films on the surface of pure Mg was about 0.4 μm. With the addition of Y-content, the oxidation film thickness increased from 0.5 μm (Mg-3Y) to more than 1.5 μm (Mg-7Y). This phenomenon was attributed to the high activity of Y element, which preferentially combines with oxygen to form oxide films (Wang et al., 2009).

As shown in **Table 6**, all the oxidation films were consisted of Y_2O_3 and MgO. For both pure Mg and Mg-xY ($x = 3, 5, 7$ wt.%) alloys, the major content of the oxidation film is MgO. However, the closer to the top surface of the oxide film, the larger amount of Y_2O_3-content. In general, the protection

TABLE 6 | The elemental composition of different cross-section locations.

Materials	Locations	Weight %		
		Element Mg *K*	Element O *K*	Element Y *K*
Mg	Spot 1	92.8	7.2	—
	Spot 2	95.2	4.8	—
	Spot 3	99.3	0.7	—
Mg-3Y	Spot 1	41.9	28.7	29.4
	Spot 2	44.8	25.7	29.5
	Spot 3	74.6	16.5	8.8
Mg-5Y	Spot 1	35.1	32.3	32.6
	Spot 2	33.6	31.4	35.0
	Spot 3	83.4	14.0	2.7
Mg-7Y	Spot 1	39.3	32.1	28.7
	Spot 2	42.2	31.4	26.3
	Spot 3	75.6	17.8	6.6

performance of oxidation products to α-Mg matrix was related the PBR of films covered on the samples, which determine the diffusion rate of metal atoms from metal/oxide interface to oxide/air interface, and the diffusion rate of oxygen atoms from oxide/air interface to metal/oxide interface (Zhao et al., 2018). The inward diffusion of oxygen atoms and the outward diffusion of Mg atoms through the oxide films was suppressed due to the compact microstructure of Y_2O_3-content.

Figure 5 shows the open circuit potential of pure Mg and Mg-xY alloys covered with oxidation films in 3.5% NaCl solution. As time increased, all the ocp values decreased, due to the desquamation of oxidation films covered on the surface of samples (Jiang, et al., 2021). The OCP value of Mg-7Y alloy was the most positive, indicating the most alleviated local corrosion of Mg-7Y alloy among the samples. In addition, with the extension of immersion time, the OCP of Mg-Y alloys tended to be stable, indicating a stabilized surface state. The electrochemical activity of the samples decreased in the order of Mg-7Y > Mg-5Y > Mg-3Y > pure Mg. The corrosion tendency of Mg-7Y was the lowest in the exposure of 3.5% NaCl for 1200s, due to the protection of the thick and compact oxidation film.

The Tafel slopes of pure Mg and Mg-xY alloys covered with oxidation films measured in 3.5% NaCl solution was shown in **Figure 6**. The corrosion reactions were identical according to the similarity of all the Tafel curves. As shown in **Figure 6**, the characteristic anode branches were generally sharp formation, which represented the dissolution of α-Mg. The cathodic hydrogen evolution was the main reaction, which determined the reaction rate of the electrochemical corrosion. When the potential was more negative than the pitting potential, the cathodic branch showed up linear Tafel characteristics. Therefore, the corrosion current density of pure Mg and Mg-xY alloys was calculated by the tangent of linear cathode branch. The results of corrosion current density were shown in the table of **Figure 6**. Due to the different resistance of oxides films to the

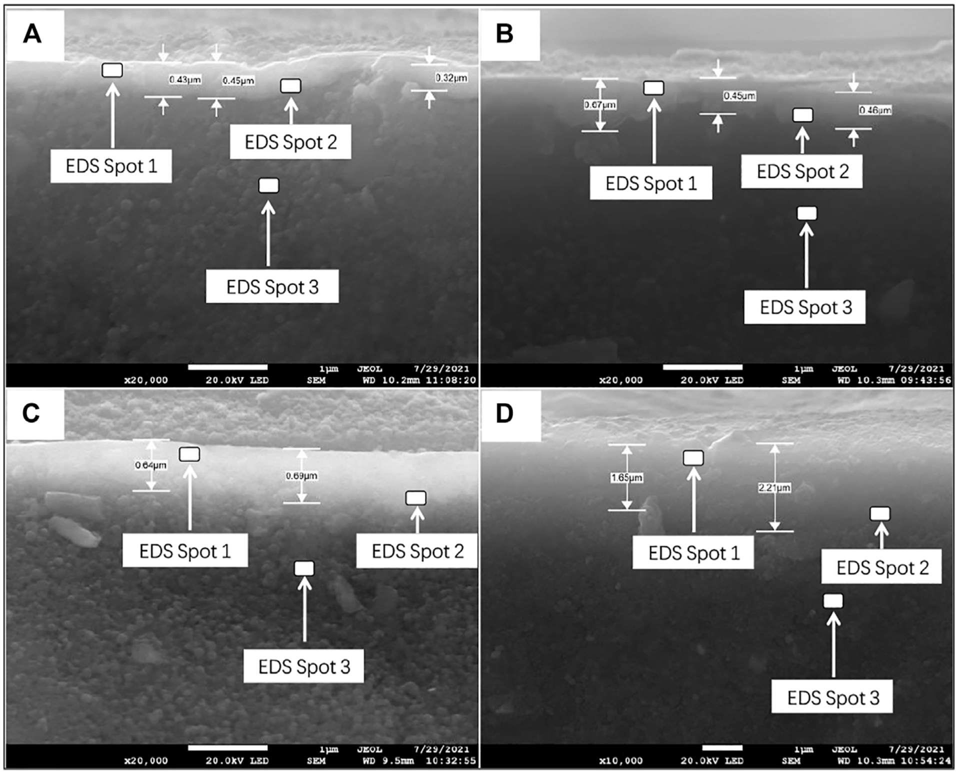

FIGURE 4 | The thicknesses of oxidation films on different samples measured by backscattered electrons: **(A)** pure Mg; **(B)** Mg-3Y; **(C)** Mg-5Y; **(D)** Mg-7Y.

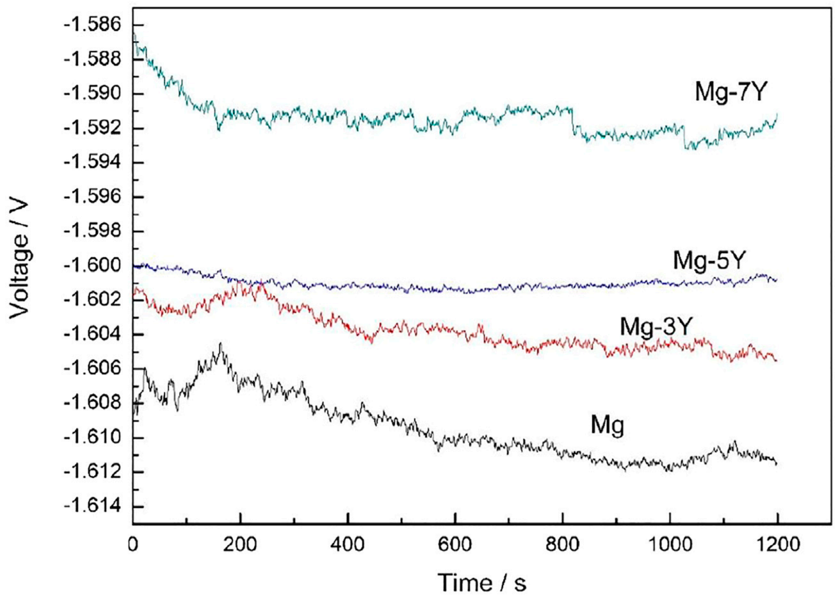

FIGURE 5 | The electrochemical open circuit potential of samples covered with oxidation films in the surface measured in 3.5% NaCl solution.

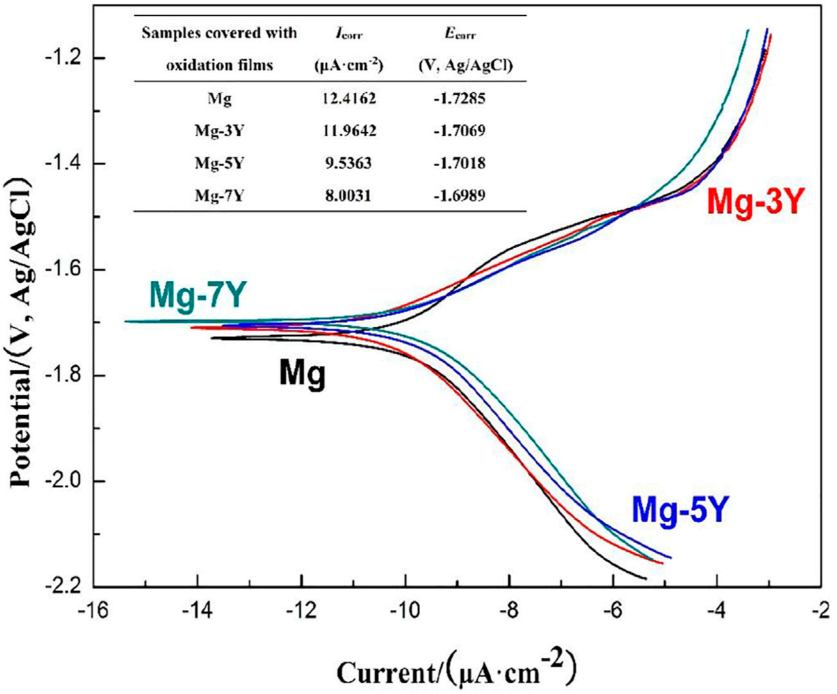

Samples covered with oxidation films	I_{corr} (μA·cm^{-2})	E_{corr} (V, Ag/AgCl)
Mg	12.4162	-1.7285
Mg-3Y	11.9642	-1.7069
Mg-5Y	9.5363	-1.7018
Mg-7Y	8.0031	-1.6989

FIGURE 6 | The electrochemical Tafel slopes of samples covered with oxidation films in the surface measured in 3.5% NaCl solution.

corrosion reaction, the pure Mg showed a largest I_{corr}, whereas the Mg-7Y alloy showed the smallest. The results depended on thickness and density of oxides films, which indicated that the oxides films formed in the surface of Mg-7Y alloy showed a best corrosion barrier effect.

The electrochemical impedance spectra curves of pure Mg and Mg-xY alloys covered with oxidation films measured in 3.5% NaCl solution was shown in **Figure 7**. The largest electrochemical impedance spectra of Mg-7Y alloy samples indicated that hydrogen evolution of the α-Mg matrix reaction had the

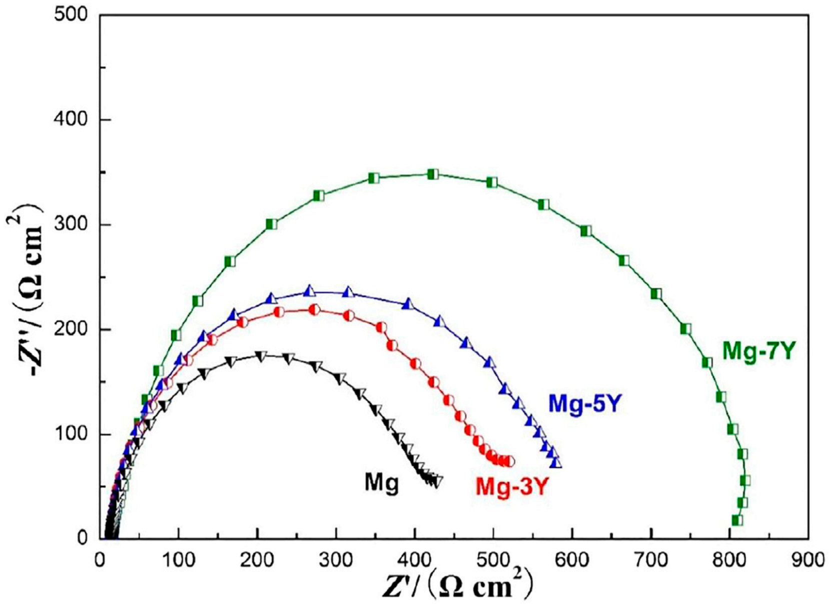

FIGURE 7 | The electrochemical impedance spectra curves of samples covered with oxidation films in the surface measured in 3.5% NaCl solution.

largest energy barrier. According to the results in **Figure 6**, the corrosion resistance can be ranked as follows: pure Mg < Mg-3Y < Mg-5Y < Mg-7Y, which demonstrated that the tendency was consistent with the preceding data in this study. The electrochemical impedance spectra curves of different samples were different, which represented distinctive dynamic corrosion process. The larger of the PBR of oxides films, the stronger of the barrier effect on the ion diffusion of corrosion reaction. Therefore, the alloy with the most Y-content showed the best corrosion resistance.

PBR is the ratio of oxide volume generated from the combination of metal and oxygen on the metal surface to the volume of consumed metal atoms, which reflects the stress condition in the oxide film. The corrosion tendency of magnesium alloy is closely related to the conditions of oxide layer during oxidation. The PBR of Y_2O_3 films generated from $Mg_{24}Y_5$ was about 1.1923, which indicated the Y_2O_3 films were continuous and compact (Okamoto, 1992). Therefore, the content of Y-content increased, the corrosion tendency of Mg-Y alloys decreased. When PBR is less than 1 or more than 2, tensile stress or excessive compressive stress exists in the oxide film, and the film is prone to rupture. The PBR value of MgO/Mg was 0.81, which indicated that the MgO layer had a large internal tensile stress, and the film structure was loose (Lin, et al., 2010; Qin, et al., 2016; Lee, et al., 2017). As a result, the pure Mg had the largest corrosion tendency than Mg-Y alloys.

As shown in **Figure 8**, the oxidation mechanism of pure Mg and Mg-Y alloys in this study. With the increasing of Y-content, the amount and volume fraction of precipitated phases on grain boundary of Mg-Y binary alloys became larger before heat treatment. After the heat treatment, pure Mg reacted with O atom to form a loose porous oxide film in **Figure 7A**. For Mg-Y binary alloys, the Y atom bonded to the O atom preferentially, and then the Mg atom bonded to the O atom at the high temperatures. The Y_2O_3 and MgO products formed in the surface of different Mg-Y binary alloys. With the increasing of Y-content, the ratio of Y_2O_3 formed in the oxides became larger. Moreover, the volume and dimensions of Y_2O_3 also showed a large improvement. As the oxidation reaction processed, the equilibrium state of the interface between the alloy and the oxidation environment changed (You, et al., 2014). At the initial stage of oxidation, the equilibrium state of the alloy interface was alloy-oxidation environment. With the formation of oxidation films, the equilibrium state of the interface changed to alloy/oxidation products/oxidation environment. During the oxidation reaction, the PBR value of MgO products was only about 0.8, which could not protect the α-Mg matrix from the further corrosion reaction effectively. However, the PBR value of Y_2O_3 was larger than 1, which improved the overall density of mixed oxide in the surface to a certain extent. Therefore, the protective effect of mixed oxide on the matrix was improved. This phenomenon indicated that the more of Y-content, the stronger the protective effect of oxide film on the α-Mg matrix.

On the other hand, precipitated phases in the magnesium alloys often act as the cathode of microelectrochemical coupling reaction, accelerating the corrosion of α-Mg matrix. With the alloying element increased gradually, more and more Y-content reacted with α-Mg matrix, the number of precipitated phases also increased tremendously. However, In the heating process, the precipitated phases containing rare earths were easier to oxidize than the magnesium matrix. And then the Y_2O_3 formed have a better protection effect on the α-Mg matrix. The more precipitated phases contained rare earth were, the more Y_2O_3 is oxidized, which resulted a improvement to the corrosion resistance of α-Mg matrix.

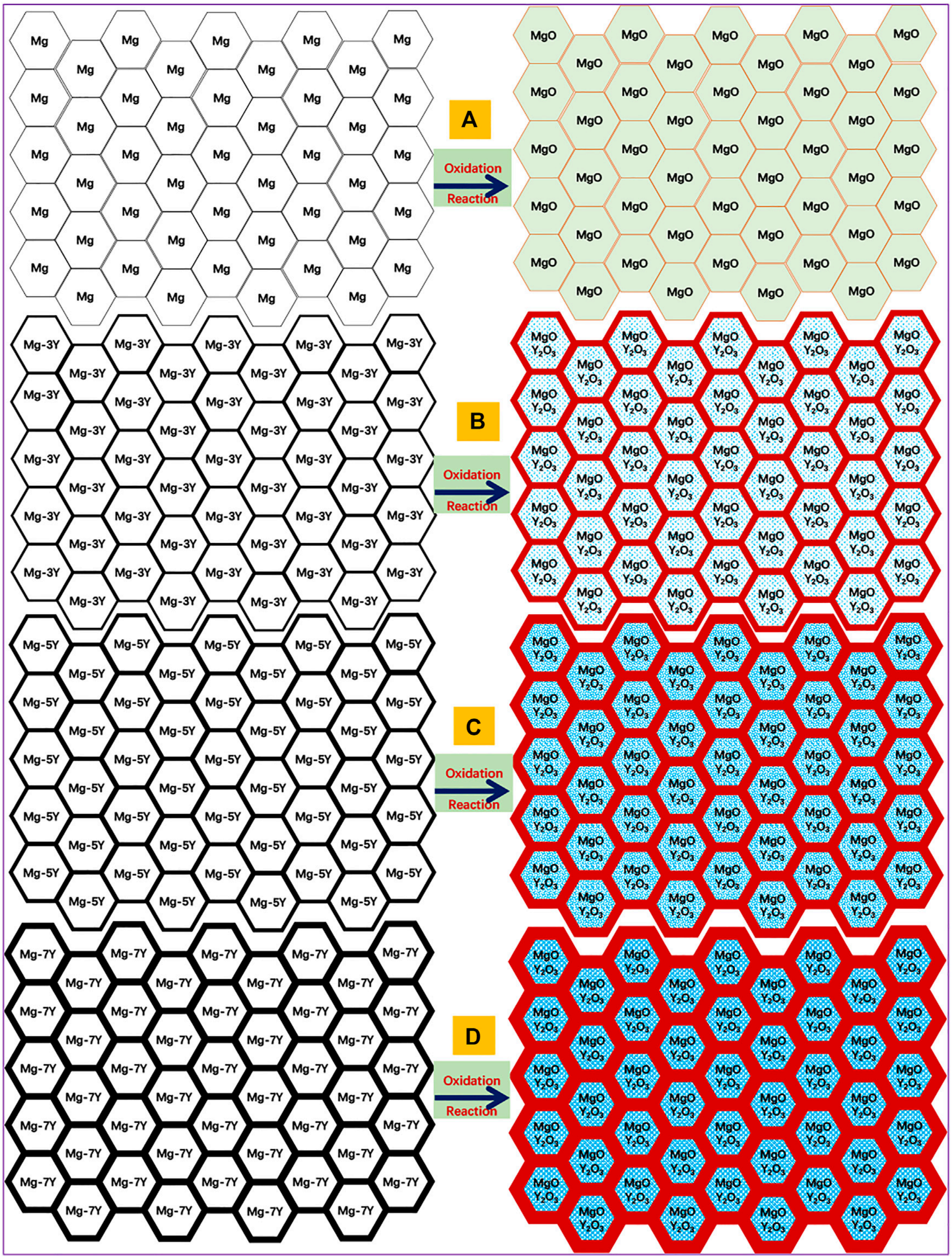

FIGURE 8 | The oxidation mechanism of pure Mg and Mg-Y alloys in this study.

In fact, different types of precipitated phases may exist in the same magnesium alloy. Moreover, one alloying element also may form different kinds of precipitated phases in the magnesium alloys with the changes of the alloying element content. In this work, the PBR values of the oxide film formed from the common precipitated phases in magnesium alloys were calculated. In the actual oxidation process of magnesium alloys, it is possible that multiple oxidation reactions occur simultaneously. This research is expected to provide guidance in the development of heat-resistant magnesium alloys by adjusting the types of alloying elements and film formation from the precipitated phases.

CONCLUSION

1) The PBR values of preferentially oxides formed from $Mg_{12}Nd$ and $Mg_{24}Y_5$ were 1.0584 and 1.1923, respectively, which indicated a good protection for the Mg matrix. The PBR values of preferentially oxides formed from Mg_3Gd and $MgNi_2$ were larger than 2, which existed a compressive stress. The PBR values of preferentially oxides formed from $Mg_{17}Al_{12}$, $MgZn_2$, $MgCu_2$, Mg_2Ca, $Mg_{12}Ce$, and MgAg were less than 1, which existed a tensile stress. Both compressive stress and tensile stress would lead the fracture of oxides. These PBR values of oxides indicated a poor protection of Mg matrix.
2) The oxide films formed on the surfaces of Mg-xY (x = 3, 5, 7 wt.%) samples were consisted of Y_2O_3 and MgO. The formation of Y_2O_3 was caused by the oxidation of $Mg_{24}Y_5$. The PBR values of preferentially oxides formed from $Mg_{24}Y_5$ was 1.1923, and then increased the PBR of MgO formed from Mg matrix to a certain extent. The electrochemical experiments proved that the corrosion resistance of Mg-Y alloys improved with the increasing of Y-content.
3) In the actual oxidation process, multiple oxidation reactions will occur simultaneously. The composition of oxide films on the surface of magnesium alloys are complex. This work is expected to give a scientific and reasonable method to improve intrinsic corrosion resistance of magnesium alloys by regulating the types of precipitates.

DATA AVAILABILITY STATEMENT

The original contributions presented in the study are included in the article/Supplementary Material, further inquiries can be directed to the corresponding author.

AUTHOR CONTRIBUTIONS

QJ and DL conceived and designed the study and experiment plan. CL performed the experiments. NL analyzed the energy dispersive spectrum datas. BH verified the experimental results. QJ wrote the paper. DL, CL, NL, and BH reviewed and edited the manuscript. All authors read and approved the manuscript.

FUNDING

The present work was supported by National Natural Science Foundation of China for Exploring Key Scientific Instrument (No.41827805) and the Open Funds of the State Key Laboratory of Rare Earth Resource Utilization (No. RERU2021017) for providing support.

ACKNOWLEDGMENTS

The authors gratefully acknowledge professor Kui Zhang of State Key Laboratory for Fabrication and Processing of Nonferrous Metals.

REFERENCES

Bradford, S. A. (1993). *Oxidation: Metal-Gas Reactions, Corrosion Control*. Boston, MA, US: Springer, 289–312. doi:10.1007/978-1-4684-8845-6_14

Chang, C. L., Lu, S., Fu, Y. Y., and Zhang, H. P. (2015). Flammability and the Oxidation Kinetics of the Magnesium Alloys AZ31, WE43, and ZE10. *Corrosion Sci.* 100, 177–185. doi:10.1016/j.corsci.2015.07.020

Cheng, S. L., Yang, G. C., Fan, J. F., Li, Y. J., and Zhou, Y. H. (2009). Effect of Ca and Y Additions on Oxidation Behavior of AZ91 alloy at Elevated Temperatures. *Trans. Nonferrous Met. Soc. China* 19, 299–304. doi:10.1016/S1003-6326(08)60268-X

Czerwinski, F. (2002). The Oxidation Behaviour of an AZ91D Magnesium alloy at High Temperatures. *Acta Mater.* 50, 2639–2654. doi:10.1016/S1359-6454(02)00094-0

Czerwinski, F. (2012). Oxidation Characteristics of Magnesium Alloys. *JOM* 64 (12), 1477–1483. doi:10.1007/s11837-012-0477-z

Czerwinski, F. (2015). The Reactive Element Effect on High-Temperature Oxidation of Magnesium. *Int. Mater. Rev.* 60 (5), 264–296. doi:10.1179/1743280415Y.0000000001

Fan, J. F., Yang, C. L., Han, G., Fang, S., Yang, W. D., and Xu, B. S. (2011). Oxidation Behavior of Ignition-Proof Magnesium Alloys with Rare Earth Addition. *J. Alloys Comp.* 509 (5), 2137–2142. doi:10.1016/j.jallcom.2010.10.168

James, G. S. (2005). *Lange's Handbook of Chemistry*. New York, NY MCGRAW-HILL, 1.238–1.279.

Jiang, Q. T., Lu, D. Z., Wang, N., Wang, X. T., Zhang, J., Duan, J. Z., et al. (2021). The Corrosion Behavior of Mg-Nd Binary Alloys in the Harsh marine Environment. *J. Magnesium Alloys* 9 (1), 292–304. doi:10.1016/j.jma.2019.12.010

Kaya, A. A. (2020). Review on Developments in Magnesium Alloys. *Front. Mater.* 7, 198. doi:10.3389/fmats.2020.00198

Lee, D. B., Abro, M. A., and You, B. S. (2017). High-temperature Oxidation of AZ91-0.3%Ca-0.1%Y alloy in Air. *Met. Mater. Int.* 23 (4), 720–725. doi:10.1007/s12540-017-6745-2

Lin, P. Y., Zhou, H., Sun, N., Li, W. P., Wang, C. T., Wang, M. X., et al. (2010). Influence of Cerium Addition on the Resistance to Oxidation of AM50 alloy Prepared by Rapid Solidification. *Corrosion Sci.* 52, 416–421. doi:10.1016/j.corsci.2009.09.029

Liu, J., Li, Y., and Wang, F. (2009). The High Temperature Oxidation Behavior of Mg-Gd-Y-Zr alloy. *Oxid Met.* 71, 319–334. doi:10.1007/s11085-009-9145-2

López, M. D., Múnez, C. J., Carboneras, M., Rodrigo, P., Escalera, M. D., and Otero, E. (2010). Influence of Temperature on Oxidation Behaviour of ZE41 Magnesium alloy. *J. Alloys Comp.* 491 (1/2), 131–136. doi:10.1016/j.jallcom.2009.10.163

Mebarki, N., Ravi Kumar, N. V., Blandin, J. J., Suery, M., Pelloux, F., and Khelifati, G. (2005). Correlation between Ignition and Oxidation Behaviours of AZ91 Magnesium alloy. *Mater. Sci. Technol.* 21, 1145–1151. doi:10.1179/174328405X58904

Medved, J., Mrvar, P., and Vončina, M. (2009). Oxidation Resistance of Cast Magnesium Alloys. *Oxid Met.* 71 (5/6), 257–270. doi:10.1007/s11085-009-9141-6

Nie, J. F. (2012). Precipitation and Hardening in Magnesium Alloys. *Metall. Mater. Trans. A* 43, 3891–3939. doi:10.1007/s11661-012-1217-2

Okamoto, H. (1992). Mg-Y (Magnesium-Yttrium). *J. Phase Equilib.* 13 (1), 105–106. doi:10.1007/BF02645395

Qin, L., Ding, J., Zhao, W. M., and Fang, Z. (2016). Oxidation Behavior and Surface Tension of Mg-1.2Ca alloy with Ce Addition. *Rare Metal Mater. Eng.* 45 (1), 23–27. doi:10.1016/S1875-5372(16)30039-X

Shi, Z. Z., Chen, H. T., Zhang, K., Dai, F. Z., and Liu, X. F. (2020). Crystallography of Precipitates in Mg Alloys. *J. Magnesium Alloys* 9 (2), 416–431. doi:10.1016/j.jma.2020.06.013

Song, X., Wang, Z. W., and Zeng, R. C. (2021). Magnesium Alloys: Composition, Microstructure and Ignition Resistance. *Chin. J. Nonferrous Met.* 31 (3), 598–622. doi:10.11817/j.ysxb.1004.0609.2021-40013

Sudholz, A. D., Gusieva, K., Chen, X. B., Muddle, B. C., Gibson, M. A., and Birbilis, N. (2011). Electrochemical Behaviour and Corrosion of Mg-Y Alloys. *Corrosion Sci.* 53 (6), 2277–2282. doi:10.1016/j.corsci.2011.03.010

Tan, Q., Atrens, A., Mo, N., and Zhang, M.-X. (2016). Oxidation of Magnesium Alloys at Elevated Temperatures in Air: A Review. *Corrosion Sci.* 112, 734–759. doi:10.1016/j.corsci.2016.06.018

Van Orman, J. A., and Crispin, K. L. (2010). Diffusion in Oxides. *Rev. Mineralogy Geochem.* 72 (1), 757–825. doi:10.2138/rmg.2010.72.17

Wang, X. M., Zeng, X. Q., Wu, G. S., Yao, S. S., and Li, L. B. (2007). Surface Oxidation Behavior of MgNd Alloys. *Appl. Surf. Sci.* 253 (22), 9017–9023. doi:10.1016/j.apsusc.2007.05.023

Wang, X. M., Zeng, X. Q., Zhou, Y., Wu, G. S., Yao, S. S., and Lai, Y. J. (2008). Early Oxidation Behaviors of Mg-Y Alloys at High Temperatures. *J. Alloys Comp.* 460 (1), 368–374. doi:10.1016/j.jallcom.2007.06.065

Wang, X. M., Wu, W. D., Tang, Y. J., Zeng, X. Q., and Yao, S. S. (2009). Early High Temperature Oxidation Behaviors of Mg-10Gd-3Y Alloys. *J. Alloys Comp.* 474 (1/2), 499–504. doi:10.1016/j.jallcom.2008.06.122

Xu, C., and Gao, W. (2000). Pilling-Bedworth Ratio for Oxidation of Alloys. *Mater. Res. Innov.* 3, 231, 235. doi:10.1007/s100190050008

You, B.-S., Park, W.-W., and Chung, I.-S. (2000). The Effect of Calcium Additions on the Oxidation Behavior in Magnesium Alloys. *Scripta Mater.* 42, 1089, 1094. doi:10.1016/S1359-6462(00)00344-4

You, B. S., Kim, Y. M., Yim, C. D., and Ha, S. K. (2014). "Oxidation and Corrosion Behavior of Non-flammable Magnesium Alloys Containing , Ca and Y," in *Magnesium Technology*. Editors M. Alderman, M. V. Manuel, N. Hort, and N. R. Neelameggham (New York, US: John-wiley), 325–329. doi:10.1002/9781118888179.ch62

Yu, X. W., Jiang, B., Yang, H., Yang, Q. S., Xia, X. S., and Pan, F. S. (2015). High Temperature Oxidation Behavior of Mg-Y-Sn, Mg-Y, Mg-Sn Alloys and its Effect on Corrosion Property. *Appl. Surf. Sci.* 353, 1013–1022. doi:10.1016/j.apsusc.2015.07.011

Yu, X., Shen, S., Jiang, B., Jiang, Z. T., Yang, H., and Pan, F. S. (2016). The Effect of the Existing State of Y on High Temperature Oxidation Properties of Magnesium Alloys. *Appl. Surf. Sci.* 370, 357–363. doi:10.1016/j.apsusc.2016.02.156

Yu, X. W., Jiang, B., He, J. J., Liu, B., and Pan, F. S. (2018). Oxidation Resistance of Mg-Y Alloys at Elevated Temperatures and the protection Performance of the Oxide Films. *J. Alloys Comp.* 749, 1054–1062. doi:10.1016/j.jallcom.2018.03.342

Zhao, X. Y., Ning, Z. L., Li, Z. Q., Zou, W. B., Li, B. H., He, K., et al. (2018). In-mold Oxidation Behavior of Mg-4.32Y-2.83Nd-0.41Zr alloy. *J. Mater. Sci.* 53 (15), 11091–11103. doi:10.1007/s10853-018-2271-y

Zhou, N., Zhang, Z. Y., Dong, J., Jin, L., and Ding, W. J. (2013). Selective Oxidation Behavior of an Ignition-Proof Mg-Y-Ca-Ce alloy. *J. Rare Earths* 31 (10), 1003–1008. doi:10.1016/S1002-0721(13)60021-6

Zhu, C. Y., and Chen, B. (2019). Atomic Scale Investigation on Precipitates and Defects of Mg-RE Alloys: a Review. *Adv. Eng. Mater.* 21 (3), 1800734. doi:10.1002/adem.201800734

Conflict of Interest: The authors declare that the research was conducted in the absence of any commercial or financial relationships that could be construed as a potential conflict of interest.